

Ellipsometric studies of synclinic and anticlinic arrangements in liquid crystal films

P. M. Johnson,¹ D. A. Olson,¹ S. Pankratz,¹ Ch. Bahr,² J. W. Goodby,³ and C. C. Huang¹

¹*Department of Physics and Astronomy, University of Minnesota, Minneapolis, Minnesota 55455*

²*Institut für Physikalische Chemie, Philipps-Universität Marburg, D-35032 Marburg, Germany*

³*School of Chemistry, The University, Hull HU6 7RX, England*

(Received 31 May 2000)

The molecular arrangements in liquid crystal freestanding films are studied when smectic C^* surface ordering occurs above the bulk smectic A to smectic C^* transition temperature. Details of the resulting structures are resolved using ellipsometry. The behavior of the film is compound dependent. Below a critical electric field, either a synclinic or anticlinic structure may be present depending on the magnitude of the bulk spontaneous polarization. A model is presented in which the low-field anticlinic arrangement results from the interaction between polarization fluctuations at the two surfaces.

PACS number(s): 61.30.Eb, 77.84.Nh, 83.70.Jr

I. INTRODUCTION

The free surface of a condensed phase can induce a phase transition that either reduces or enhances the degree of order at the surface [1]. The solid-air interface generally induces surface disorder. By contrast, several soft condensed-matter systems and liquids show increased order at the free surface. Studies of liquid crystals have shown that a free surface may raise the surface freezing temperature near a wide variety of bulk phase boundaries [2,3]. One example of surface induced freezing occurs in the liquid crystal smectic phases. These phases are characterized by a layered ordering of the constituent anisotropic molecules with no long-range positional ordering within the layer planes. In the higher temperature smectic A (SmA) phase, the average orientation of the long molecular axes (described by a unit “director” \hat{n} [4]) is parallel to the layer normal (\hat{z}). In the lower temperature smectic C phase (SmC or SmC^* for chiral compounds) the molecules tilt with respect to the layer normal. A free surface can induce tilt, causing the SmC^* phase to grow from the free surface into the SmA bulk as the SmA - SmC^* transition temperature is approached from above [5–7].

In this paper, we report our investigation of the molecular arrangements in freestanding liquid crystal films when a surface induced SmC^* phase occurs in the bulk SmA temperature window. The close proximity of the two surface structures (≥ 6 nm) gives rise to a variety of interactions and new phenomena. In the bulk SmC^* arrangement the molecules tilt in the same direction from layer to layer, with the relative azimuth modulated only by a long (~ 100 layers) pitched helix. Thus one might expect that as the SmC^* phase grows at the surface of a SmA film, the interaction between the two surface phases would promote a synclinic director profile in which the tilt direction is the same throughout the film [Fig. 1(a)]. However recent studies of thin (6–100 nm) SmA films with surface SmC^* layers have shown that the director may tilt in opposite (anticlinic) directions [Fig. 1(b)] [8–10]. Additional forces specific to the thin sample geometry must be considered to explain this anticlinic structure.

Two recent studies have proposed different mechanisms for the existence of the observed anticlinic structures in free-

standing films. Andreeva *et al.* [8] have modeled the anticlinic structure resulting from an interaction between the surface polarization and an applied field. Two polarization vectors characterize the surface polarization. The ferroelectric polarization per unit volume (\mathbf{P}_{fe}) arises from the symmetry of the bulk SmC^* phase [11]. It grows in proportion to the tilt angle [$\theta = \arccos(\hat{n} \cdot \hat{z})$] in a direction perpendicular to the tilt plane. The magnitude of \mathbf{P}_{fe} is compound dependent. The flexoelectric polarization (\mathbf{P}_{fl}) [4] is not an inherent property of the bulk phase but instead arises from the broken symmetry at each surface. \mathbf{P}_{fl} increases with the gradient in the tilt and lies in the tilt plane. The model proposes that the coupling between the electric field and the larger of these two vectors determines whether the structure is synclinic and anticlinic. While this model seems to provide a unified picture for the empirical results seen in Refs. [8,9] it cannot explain the more recent studies by Link *et al.* [10]. They observed anticlinic structures even when no external field is applied. This result suggests that a force intrinsic to the freestanding film system drives the structure into the anticlinic arrangement. To the best of our knowledge no explanation for this force has been given.

In this paper we explore the controllable parameter space of these structures in more detail than previously reported in order to explain the relevant interactions. There are at least four controllable parameters that determine whether the film takes a synclinic or anticlinic arrangement. These are temperature, film thickness, applied field magnitude, and the compound characteristics. We show that the previously reported behaviors are reproducible but compound dependent. The behavior described in Refs. [8,9] is reproduced when the compound has a relatively small saturation values of \mathbf{P}_{fe} . Compounds with large \mathbf{P}_{fe} show the behavior described by Link *et al.* The results suggest that high surface polarization leads to anticlinic structures even in the absence of an electric field. In the analysis section we present an electric field vs temperature phase diagram in which the two types of behavior are clearly distinguishable. In the discussion section we propose that the relevant long-range interaction that drives the high \mathbf{P}_{fe} compounds into the anticlinic structure arises from thermal fluctuations in the polarization field [12].

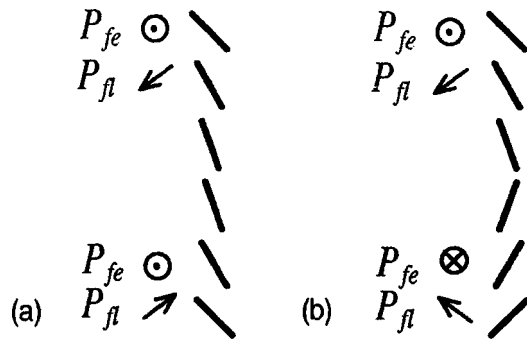


FIG. 1. Cartoon of the synclinic (a) and anticlinic (b) arrangements. In the synclinic arrangement, the surface flexoelectric polarizations cancel each other, leaving a net ferroelectric polarization perpendicular to the tilt plane. In the anticlinic arrangement the surface ferroelectric polarizations cancel each other leaving a net flexoelectric polarization in the tilt plane parallel to the smectic layers.

A model is presented that provides reasonable quantitative estimates of the magnitude of this effect.

Long-range forces in chiral tilted smectics are inherently difficult to measure and poorly understood. Yet they are thought to be vital for understanding the causes of frustration in the smectic ferroelectric phases [13]. The phenomena presented here provides evidence for a long-range force due to fluctuations in the polarization field. The freestanding film geometry proves to be an interesting means of exploring such polarization interactions.

II. EXPERIMENTAL APPROACH

The freestanding films are created by pulling a small amount of the liquid crystal material across an approximately 0.5-cm-diameter circular opening in a glass coverslip. These films are created in a sealed temperature regulated (resolution 0.01 K) environment of helium. In the absence of an external field, domains in the plane of the film will slowly rotate due to thermal fluctuations. The orientation and size of these domains can be easily observed during experimental runs using depolarized light microscopy. An electric field (E) applied in the plane of the film produces an aligned, virtually monodomain structure. Eight electrodes that surround the opening allow for the smooth reorientation of this external field. The structure may be reoriented under small applied fields (as little as $E=0.3$ V/cm) while maintaining a monodomain sample. In order to test the effect of the field magnitude on the structure we allow the field to vary from $E=0$ to $E=320$ V/cm. In the case of high applied electric field (>20 V/cm), a rectangular hole with two electrode strips is used.

The main probe used to resolve the structure of these films is null transmission ellipsometry. The main features of the approach used are described in a recent paper [14]. Polarized 633 nm laser light passes through the film at a 45° angle with the film normal. The two ellipsometric parameters Δ and Ψ , measured in the polarizer-compensator-sample-analyzer (PCSA) configuration, describe the effect of the film on the beam ellipticity and orientation, respectively [14,15]. At null, Δ is the phase lag between the p and s components of polarization as the beam enters the sample,

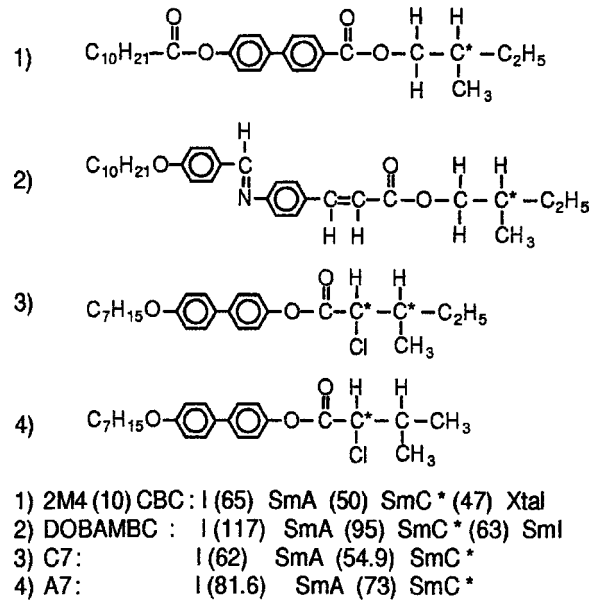


FIG. 2. Compound diagrams and phase sequences. Transition temperatures are given in $^\circ\text{C}$.

and Ψ is the orientation of the output linear polarization state. The expected values of Δ and Ψ depend on the type of structure in the film as well as its orientation. By fitting a range of intensities about the null point, a resolution of 0.001° in Δ and Ψ is achievable at an acquisition rate of 1 point/min. In order to eliminate window effects without compromising the necessary dry environment, the polarizer, compensator, and analyzer are enclosed within the sealed helium environment. Insulating walls thermally isolate the optical components from the film oven and prevent temperature-induced variations in the component properties. Two 2 mm apertures separate the polarization optics from the film minimizing convective heat transfer.

Studies were performed on five different compounds: 2M4(10)CBC, DOBAMBC, C7, chiral A7 (LA7), and a racemic mixture of A7 (50/50 LA7 and DA7 to within $<0.5\%$). Figure 2 gives the structures and transition temperatures of the compounds. All show the bulk phase sequence: Isotropic (I)-SmA-SmC* when decreasing their temperatures. From their molecular structure and direct measurements [16] 2M4(10)CBC, DOBAMBC, and the A7 racemic mixture are expected to have relatively weak values of P_{fe} (≤ 50 $\mu\text{C}/\text{m}^2$) compared to C7 and LA7 (≈ 1.5 mC/m^2) [17]. C7 and A7 show a strongly first-order SmA-SmC* bulk phase transition. To minimize the effect of impurities, each compound was recrystallized prior to use. Since the behavior of the weakly ferroelectric compounds was fundamentally different from that of the strongly ferroelectric compounds, we refer to these two groups of compounds as group A and group B, respectively. Compounds with no bulk antiferroelectric or ferroelectric phases were chosen in order to simplify the consideration of possible causes of the anticlinic arrangement [18].

For all of the compounds studied, the layer thickness (d), number of layers (N), and the ordinary (n_o) and extraordinary (n_e) indices of refraction were determined at high temperatures in a SmA window by spreading 20–30 films of thickness from 2 to ~ 100 layers and fitting the resulting Δ

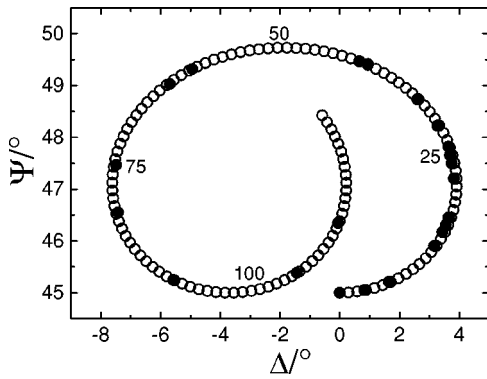


FIG. 3. Determination of n_0 , n_e , and d for the compound LA7. The data (solid circles) are obtained by spreading 20 films of thickness varying from 3 to 116 layers. The fit (open circles) gives $d = 24.6$ Å, $n_0 = 1.487$, and $n_e = 1.605$. The locations of several thicknesses are marked in the plot.

vs Ψ curve to a uniaxial slab model. The shape of the curve can be fitted by varying the indices of refraction. Once the experimental and theoretical curves are matched up, the layer thickness d can be varied until each point in the theoretical curve matches one of the experimental points. This approach is similar though slightly more efficient than a previous method [19]. The data and fit for one compound is shown in Fig. 3. This also allows for the determination of the number of smectic layers in the film to within one layer.

One of the main goals of these experiments was to locate the transitions between synclinc and anticlinic arrangements as functions of temperature, film thickness, and field strength. To this end, temperature ramps were performed on each compound at a variety of field strengths and film thicknesses. During these temperature scans, the field orientation was fixed perpendicular to the optical plane of incidence. Cooling and heating runs were performed through the entire SmA temperature range after which the sign of the field was reversed and the ramps repeated. Unless otherwise noted, the ramp rates were 0.1 K/min. Fields ranging from 0.3 to 320 V/cm were applied with films varying in thicknesses from 2 to 60 layers. The temperature at which the structure changes between the synclinc and anticlinic arrangements (T_{tr}) can be clearly resolved as a step in the otherwise smooth evolution of Δ and Ψ . Since the synclinc and anticlinic structures are expected to have different effects on Δ and Ψ under field reversal, the two structures can easily be differentiated [9].

A second goal was to unequivocally establish the molecular arrangement at $E=0$. This information is of particular importance because one previous model [8] cannot explain anticlinic structures at $E=0$. Since previous studies have required an aligning field to differentiate the two structures, and small electric fields can often induce a change from one structure to the other, a new technique was needed to address this question. To this end, each film was cooled from the high end of the SmA phase to several temperatures of interest at $E=0$. Δ vs Ψ curves were then obtained with no applied field by allowing the film to be rotated randomly due to thermal fluctuations. The shape of these curves allowed for the two structures to be clearly differentiated at $E=0$. Often the film was allowed to reorient randomly at $E=0$ for

several hours to assure that the observed structure was not a metastable state.

Following these random rotations at $E=0$, rotations were carried out at $E>0$. This served two purposes. First, knowledge of the ellipsometric parameters as a function of orientation allows for specific models of the molecular arrangement to be tested in more detail than previously explored [9,18]. As will be shown in the analysis section, additional details about the synclinc and anticlinic arrangements can be resolved using this technique. Second, field ramps allowed for observation of transitions between synclinc and anticlinic structures driven by a change in field magnitude rather than a change in temperature. The rotations were carried out in 6° steps at a rate of 1 step/min.

III. RESULTS

The group A compounds show a discrete switch from anticlinic to synclinc structure upon cooling. The most extensive temperature ramps were carried out on the compound 2M4(10)CBC at the two different field orientations and at a number of field strengths. Shown in Fig. 4(a) are temperature ramps at ± 4 V/cm for a 33L film of 2M4(10)CBC (open and closed symbols for + and $-E$, respectively). The steps in Δ and Ψ that occur within the bulk SmA window indicate a sudden change in the film structure. When the field is reversed at a given temperature, there is a larger change in Ψ and smaller change in Δ in the high-temperature ($\geq 53.5^\circ\text{C}$) state than the low-temperature ($\leq 52.5^\circ\text{C}$) state. As will be shown below, this suggests that the arrangement is anticlinic at higher temperatures and synclinc at lower temperatures. The temperature-induced change between the two structures was discrete at these field strengths. No obvious intermediate structures were observed. This result is similar to that seen in Ref. [9]

The group A compounds also showed a field-dependent hysteresis. For the film in Fig. 4(a), at $E = \pm 4$ V/cm, T_{tr} is approximately 1 K lower when cooling than when heating. In other words, the width of the hysteresis region ΔT_{tr} , is 1 K. Figure 4(a) also shows results at a reduced field strength of 0.3 V/cm (dashed lines). As seen in the plot, lowering E caused T_{tr} to decrease when cooling and increase when heating such that $\Delta T_{tr} \cong 5$ K. Temperature ramps were repeated on this film with applied fields from 0.3 to 320 V/cm. ΔT_{tr} decreased monotonically with increased voltage. Qualitatively similar results were seen in DOBAMBC and racemic A7. At voltages above 80 V/cm, the transition became smeared out over $\sim 1/2$ K during both heating and cooling suggesting that the film occupied some intermediate states during the transition.

T_{tr} is plotted for 2M4(10)CBC as a function of voltage for the heating and cooling runs in Fig. 5. ΔT_{tr} shrinks to unmeasurably small values at high fields. T_{tr} also converges to a roughly field-independent value at fields above 20 V/cm. The error bars on the points at 160 and 320 V/cm convey the increased width of the transition region observed at these high voltages. The inset of Fig. 5 shows the inverse relationship between the field strength and the size of the hysteresis region $\Delta T_{tr} \propto 1/E$, for the two decades bounded by $0.8 \text{ V/cm} \leq E \leq 80 \text{ V/cm}$. Data for the fields higher than 80 V/cm are excluded from this plot due to the smearing of T_{tr} .

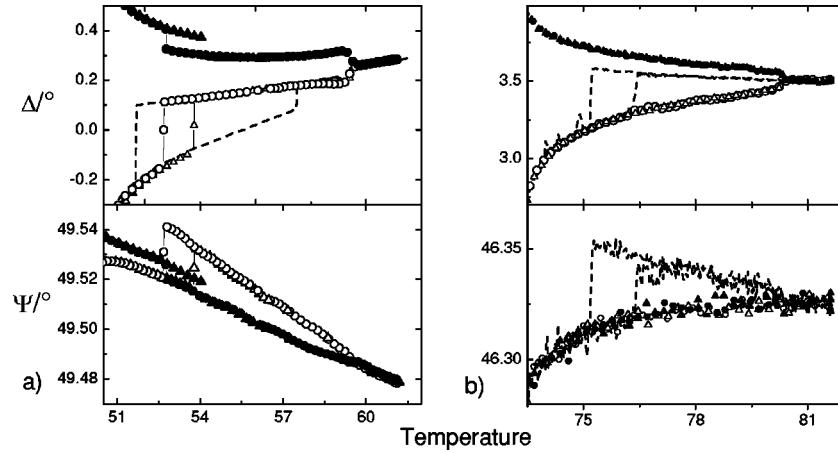


FIG. 4. Temperature ramps for (a) the group A compound 2M4(10)CBC ($N=33$) at $E = \pm 4$ V/cm (symbols) and 0.3 V/cm (dashed lines) and (b) the group B compound LA7 ($N=16$) at $E = \pm 10$ V/cm (symbols) and 0.5 V/cm (dashed lines). The open symbols are at $+E$ while the closed are at $-E$. Circles denote cooling, triangles heating. Only the $+E$ case is depicted for the low-field ramps (dashed lines) to retain visual clarity. For both compounds, if an anticlinic state is present, it occurs at the high-temperature side of the ramp. In (b), this state exists only at low fields.

The group B compounds showed a temperature-induced transition from anticlinic to synclinic only at low fields. Such a transition is shown for a 14 layer LA7 film at $E = 0.5$ V/cm in Fig. 4(b) (dashed lines). Only one field orientation is shown here for visual clarity, but it was determined that the high-temperature ($\geq 77.5^\circ\text{C}$) state was anticlinic and the low-temperature state ($\leq 75.5^\circ\text{C}$) synclinic with $\Delta T_{tr} \cong 2$ K. When E was increased to 1 V/cm and then 5 V/cm, T_{tr} increased for both heating and cooling while ΔT_{tr} decreased somewhat. At $E \geq 10$ V/cm the anticlinic structure did not appear at all in the SmA phase window. The temperature ramp showing no anticlinic structure at $E = 10$ V/cm is shown in Fig. 4(b) (open and closed symbols for $+$ and $-E$, respectively). C7 showed similar behavior, although the SmA surface layers persisted up to the isotropic transition temperature at which point the film pops. Thus unlike in the group A compounds, increasing the field reduces the temperature window for the anticlinic structure both on heating and cooling. A high enough field eliminates the anticlinic structure all together.

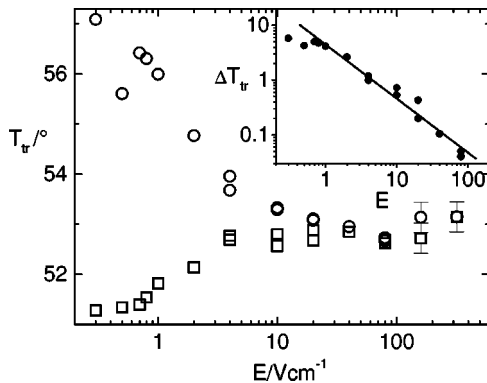


FIG. 5. The transition temperature between the synclinic and anticlinic structure (T_{tr}) vs the applied field strength for a 33-layer 2M4(10)CBC film for cooling (open squares) and heating (open circles). The size of the hysteresis region ΔT_{tr} is plotted vs E on the log-log plot in the inset. The slope of the linear fit is 0.98 ± 0.05 over two decades.

At zero and low external fields, for all the variations of thickness and temperature studied, the $E=0$ state of the system was found to be synclinic for all of the group A compounds. This result is shown for two thicknesses of 2M4(10)CBC in Fig. 6(a). Two characteristic shapes in the Δ vs Ψ plot are observed. The zero- and low-field shapes show a wide span in Δ and a roughly concave down orientation (open circles). The high-field shape shows a wider span in Ψ and a concave right orientation (solid circles). Also shown are fits to simulations for the synclinic and anticlinic structures. The field required to switch from synclinic to anticlinic increased with decreasing film thickness and decreasing temperature. The structure can be switched back and forth between the two structures by varying E . At certain thicknesses, there is considerable hysteresis in E . For all variations of temperature and thickness, a change in structure from anticlinic to synclinic could be induced in the group A compounds by *increasing* the field.

The above results for the group A compounds may be compared with the results for the group B compounds. The C7 and LA7 compounds were examined in the high-temperature region of the SmA range for films of thickness from 3 to 30 layers. At 60.1°C , C7 showed a synclinic structure for thicknesses up to 12 layers with no applied field. For fields up to 30 V/cm, the structure in these thin films showed no switch to the anticlinic state. In films thicker than 12 layers, the $E=0$ structure was anticlinic. This can be seen in the zero-field (open triangles) and low-field ($E=1.4$ V/cm, open circles) Δ vs Ψ plots in Fig. 6(b). Anticlinic structures were also seen in the LA7 films at $E=0$ and $N > 7$. For all of the films that show a zero-field anticlinic structure, the structure changed to synclinic with the application of a large enough field. In the group B compounds, synclinic to anticlinic transitions could be induced only by *decreasing* the applied field.

IV. DATA ANALYSIS

At null, the PCSA system can be described using the Jones matrix formalism by the following equation:

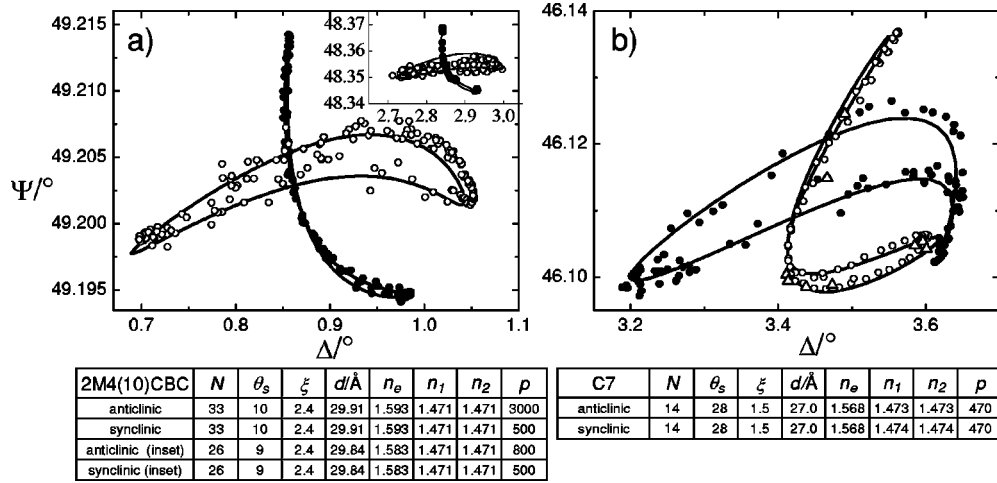


FIG. 6. Data (symbols) and fits (solid lines) for rotations in the low-or zero-field (open circles and triangles) and high-field (solid circles) states. The concave down curves showing a wide span in Δ are fit to the synclinc profile while the concave left curves are fit to the anticlinic profile. Nearly identical parameters are used for both profiles in each film. (a) 2M4(10)CBC ($T=56^\circ\text{C}$): The main plot shows curves created with rotating fields of 0.4 V/cm (open circles) and 2 V/cm (solid circles) on an $N=33$ film. The inset shows plots at zero field and 1 V/cm field for an $N=26$ film. The multiple orientations obtained for the curves in the inset occur due to thermally induced reorientations at $E=0$. The high-field state in the inset was obtained just after the field was turned off during the roughly 10 min that the film remained in the metastable high-field state. After 10 min., the film settles into the $E=0$ state. (b) C7 ($T=60.1^\circ\text{C}$): Rotations at 1.4 V/cm (open circles) and 7.1 V/cm (solid circles) on an $N=14$ film. Also included are several points taken at $E=0$ (open triangles). The parameters used to fit to the data are given for both plots. The uncertainty in these parameters is described in the text.

$$\left| R(\Psi) \begin{pmatrix} 1 & 0 \\ 0 & 0 \end{pmatrix} R(-\Psi) \begin{pmatrix} T_{11} & T_{12} \\ T_{21} & T_{22} \end{pmatrix} \begin{pmatrix} 1 \\ e^{i\Delta} \end{pmatrix} \right|^2 = 0. \quad (1)$$

$$\Psi = \arctan \left(\frac{T_{11} + T_{12}e^{i\Delta}}{T_{21} + T_{22}e^{i\Delta}} \right) \pm \frac{\pi}{2}. \quad (3)$$

The vector on the right describes the polarization state entering the sample, where $\Delta = 90^\circ - 2P$ and P is the polarizer orientation [15]. T_{ik} is the transmission matrix of the sample. The three terms on the left describe the effect of the analyzer oriented at angle Ψ , where R is the rotation matrix. The left-hand side of Eq. (1) is the transmitted intensity of the system that equals zero at null. Predicting the values of Δ and Ψ for a given film structure reduces to finding T_{ik} for a theoretical structure and solving the above equation for Δ and Ψ . Note that the definitions of Δ and Ψ given by Eq. (1) are more general than those given when the reference frame that diagonalizes T_{ik} is known *a priori* [15]. The elements of the transmission matrix can be generated numerically using the 4 by 4 matrix method for stratified media [20]. The routine assigns to each layer (indexed by j) an ellipsoid of refraction that approximates the average effect of the molecules on the polarization state of light. The ellipsoid principal axes are oriented such that n_e , n_1 , and n_2 give the magnitudes of the components of this ellipsoid in the \hat{n} , $\hat{n} \times \hat{z}$, and $\hat{n} \times (\hat{n} \times \hat{z})$ directions, respectively. The orientation of the long axis of this ellipsoid in the j th layer can be described by the tilt angle θ_j and the azimuthal angle ϕ_j .

For a nondiagonal transmission matrix, Eq. (1) can be solved analytically for Δ and Ψ giving the following results:

$$\Delta = \arg(T_{11}T_{22}^* - T_{12}^*T_{21}) + \arcsin \left(\frac{\text{Im}(T_{11}T_{21}^* + T_{12}T_{22}^*)}{|T_{11}T_{22}^* - T_{12}^*T_{21}|} \right), \quad (2)$$

Equations (2) and (3) apply under the assumption of perfect optical components. For imperfect optical components, the expected values of Δ and Ψ can be solved numerically for a given T_{ik} . However, the deviation from ideal of the optical components used in these experiments was determined to be sufficiently small to allow Eqs. (2) and (3) to be used. Using the expressions in Eqs. (2) and (3), the values of Δ and Ψ were calculated for trial $[\theta]$ and $[\phi]$ profiles for all orientations of the structure with respect to the incident beam.

While the synclinc or anticlinic nature of the structures are easily distinguishable from the observed shape of the Δ vs Ψ curve, fitting to the details of this shape reveals additional information about the structure. The films are assumed to possess a surface tilt (θ_s). The tilt angle decreases monotonically as it penetrates into the film over a depth ξ (given here in units of layer thickness). The expected Δ vs Ψ curve is somewhat insensitive to the exact functional form of this decrease. However fits to a step function model were qualitatively worse than a model in which the tilt decays exponentially from the surface. The fits are sensitive to the magnitudes of θ_s and ξ together, although there is a strong covariance between the two parameters. Fits in which the integrated tilt was a free parameter showed lower variance in this parameter ($\sim 20\%$) than those obtained for θ_s and ξ . Thus the fits give an accurate measure of the integrated tilt near the surface of the film while the uncertainties in θ_s and ξ are fairly large. This result reflects the fact that the wavelength of light is much longer than the layer thickness and is thus more sensitive to properties of the entire surface region than to details of the region.

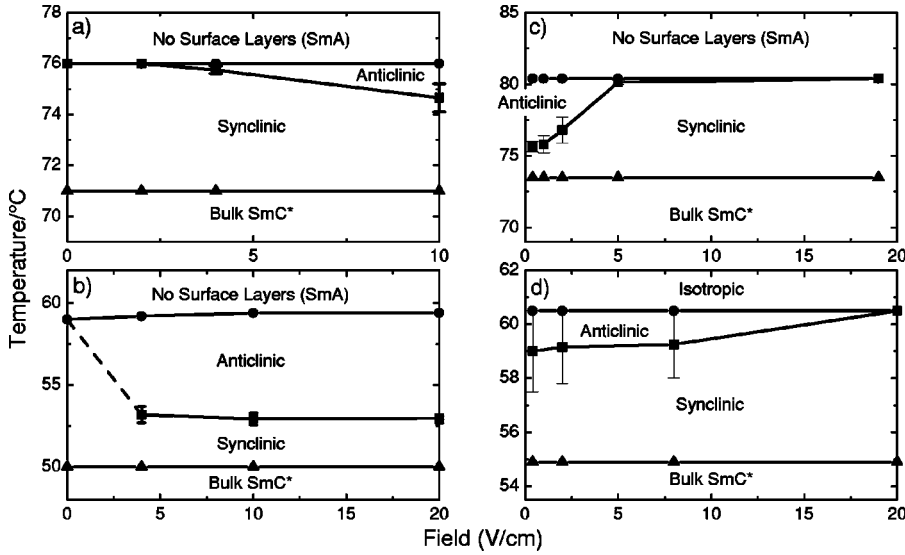


FIG. 7. Temperature vs field phase diagram for the compounds studied. On the left are the group A compounds: (a) racemic A7, $N = 17$, and (b) 2M4(10)CBC, $N = 33$. On the right are the group B compounds: (c) LA7, $N = 17$, and (d) C7, $N = 14$. The error bars convey ΔT_{lr} due to hysteresis. The dashed line in (b) covers the region of increasing hysteresis for 2M4(10)CBC. The zero-field rotation point for this compound was taken carefully using $E = 0$ rotation data over the entire temperature range.

The fits presented in Fig. 6 use the following functional form for θ_j : $\theta_j = \theta_s \cosh(j/\xi) / \cosh(N/2\xi)$ for the synclinic structure and $\theta_j = \theta_s \sinh(j/\xi) / \sinh(N/2\xi)$ for the anticlinic structure. The layer index j here varies from $-N/2$ to $+N/2$. The $[\phi]$ profile is modeled by assigning a long pitch (p layers) to the structure, i.e., $\phi_j = j * 360/p$. The orientation of the structure with respect to the field was determined by its symmetry. The tilt plane of the synclinic structure is perpendicular to E while the anticlinic tilt plane is parallel to E [8–10]. The orientation in the fits was set to these values and only allowed to float within the angular resolution of the experiments ($\approx 5^\circ$). As described above, the thickness and two indices of refraction are determined prior to modeling in the SmA phase. The symmetry of the tilted smectic phases allows for a biaxial ellipsoid of refraction. However the symmetry of the molecule and high rotational invariance about the molecular long axis suggest $n_1 \approx n_2 \approx n_0$. The indices of refraction and layer thickness will be slightly temperature dependent. To account for this, d , n_e , n_1 , and n_2 are allowed to float during the fit, but are ultimately compared with the SmA values to test the validity of the results. Data for the low-field and $E = 0$ states had less well-defined orientations. For this reason, the least-squares fitting was carried out on the high-field state first.

The values of the parameters obtained from the fits are given in the table in Fig. 6. Those parameters that can be compared with their SmA values are physically reasonable: $|n_{1,2} - n_{0\text{SmA}}| \leq 0.01$, $|n_e - n_{e\text{SmA}}| \leq 0.02$, $|n_1 - n_2| \leq 0.001$, and $|d - d_{\text{SmA}}| \leq 0.5 \text{ \AA}$. The variances on these parameters was ~ 0.01 for n_e , ~ 0.01 for $n_{1,2}$, and $\sim 0.5 \text{ \AA}$ for d . In general, the high covariance's with this number of parameters is expected to be a more likely source of error. The parameters used to fit both the anticlinic and synclinic data are the same for each film except for a slight change in pitch. This change in pitch is not physically unreasonable since the chiral interaction at an anticlinic layer interface is expected to be different from that at a synclinic layer interface. The fits also allow for the calculation of the surface polarization and the tilt angle at the center of the film. These values will be calculated and used in the discussion section.

Knowledge of the molecular arrangement acquired from the temperature ramps and electric-field rotations allows for

a phase diagram to be assembled that summarizes the dependence of the structure on the magnitude of the field and the temperature. This is shown in Fig. 7. In the group A compounds [Figs. 7(a) and 7(b)] the window for the anticlinic structure closes at low external fields over the entire temperature range. In other words, an external field is required to produce the anticlinic arrangement. By contrast, the group B compounds [Figs. 7(c) and 7(d)] show the anticlinic window opening up at low fields in the high-temperature side of the bulk SmA window. The application of a field in these compounds actually destroys the anticlinic arrangement. A comparison of Figs. 7(a) and 7(c) gives a particularly clear indication of the effect of increased P_{fe} . Both phase diagrams describe the behavior of a 17 layer A7 film. Figure 7(a) shows the results for the racemic mixture (group A). Figure 7(c) shows those for LA7 (group B). One can conclude that increasing P_{fe} fundamentally changes the behavior.

V. DISCUSSION

For all of the compounds, the existence of hysteresis in the switch between synclinic and anticlinic arrangements along with the fact that no intermediate states are seen, suggests that the two arrangements sit in sharp local minima of the free energy over a wide temperature range. There must be a strong free-energy cost for inducing a small twist in either the synclinic or anticlinic structures. Once the barrier to twisting has been exceeded, the structure may quickly switch between the two states. This behavior is observed in both the temperature ramps and on increasing E at a fixed temperature. Such behavior has been noted previously including in recent studies of SmC films [21].

The results for the group A compounds follow the predictions of the model proposed in Ref. [8]. In this model, the synclinic structure at $E = 0$ arises from the same interactions that lead to the bulk SmC* phase. Anticlinic ordering is caused by the coupling between E and \mathbf{P}_{fl} when $P_{fl} > P_{fe}$. Sufficiently low fields reduce this coupling energy and allow the structure to return to its elastically favored synclinic state. At low enough temperatures $P_{fl} < P_{fe}$ and the structure again favors the synclinic arrangement even at large E . Providing the field is large enough to overcome the elastic bar-

rier between the two states, this model predicts that the T_{tr} will be independent of E . This qualitatively explains Fig. 5. At low fields, there is a large hysteresis because the field does not overwhelm the elastic barrier. As the field is increased, T_{tr} converges to a single value, the temperature at which $P_{fl} = P_{fe}$.

The group B compounds contradict this model. The behavior of T_{tr} is highly field dependent. As the field is increased, T_{tr} increases. At high enough applied fields, the structure assumes a synclinc arrangement at all temperatures. This can be explained by the fact that $P_{fe} \gg P_{fl}$ at all temperatures due to the large spontaneous polarization of the group B compounds. However the above model requires $P_{fe} < P_{fl}$ for an anticlinic structure to appear at all! The presence of an anticlinic state at $E=0$, as seen in Figs. 6(b) and 7(c) and 7(d) is also inconsistent with the above model. Thus a new explanation is needed for the anticlinic structure in the group B compounds at $E=0$.

The most obvious difference between group B and group A is in P_{fe} . Building on this fact, the stabilization of the anticlinic arrangement can be explained in terms of a free-energy cost due to fluctuations in P_{fe} . As will be shown below, for a strong surface polarization, this energy cost can be large compared to the interaction of the polarization with typical electric fields used in the paper. The effect can be understood qualitatively. In the synclinc arrangement, there is a net polarization/area. Thermally induced fluctuations in the plane of the film in which both surfaces fluctuate together will be damped by the interaction between the induced polarization charges. The damping is less in the anticlinic state because the polarization induced charges at the two surfaces are of opposite sign. The excess damping in the synclinc state causes the anticlinic state to be both entropically and energetically favored. While fluctuations in which the gradient at the two surfaces are of opposite sign cause an equally unfavorable charge distribution in the anticlinic state, such fluctuations are damped in both synclinc and anticlinic arrangements by the large elastic cost of twist. The proposal that antialigning forces arise from the interaction of fluctuations in the spontaneous polarization fields was used by Bruinsma and Prost [12] to explain the long-range interactions that lead to frustration in the ferrielectric phases.

To describe this interaction quantitatively we assume a two-slab model. The Hamiltonian is a version of that proposed in Ref. [12], simplified here to allow the determination of an exact expression for the free energy. The physical properties of each half of the film are described by a orientation field with both elastic and electrostatic energy costs to fluctuations. The orientation of the average polarization at position r is given by the angle $\Phi_{1,2}(r)$. The magnitude of the polarization/area of each slab is given by $P \approx \xi P_{fe} d$. Fluctuations are assumed to be small and in the x direction on average. Under this assumption, the induced charge/area in each slab is given by $P \partial_x \Phi_{1,2}$. In the anticlinic arrangement the gradient induced charge is of opposite signs for the top and bottom slabs. The two slabs are coupled in two ways. There is a energy cost for twist in the structure, i.e., when $\Phi_1(r) \neq \Phi_2(r)$. There is also an electrostatic interaction between the polarization-induced charges of the slabs. These considerations lead to the Hamiltonian

$$\begin{aligned} H_{\pm} = & \frac{1}{2} \int dx dy \sum_{k=1,2} K_{\parallel} [\nabla \Phi_k(r)]^2 \\ & + \frac{1}{2} \int dx dy K_{\perp} \left(\frac{\Phi_1(r) - \Phi_2(r)}{l} \right)^2 \\ & + \frac{P^2}{2\epsilon} \int dx dy dx' dy' \sum_{k=1,2} \frac{\partial_x \Phi_k(r) \partial_x \Phi_k(r')}{|r-r'|} \\ & \pm \frac{P^2}{2\epsilon} \int dx dy dx' dy' \frac{\partial_x \Phi_1(r) \partial_x \Phi_2(r')}{\sqrt{(r-r')^2 + l^2}}. \end{aligned} \quad (4)$$

The first and second terms give the elastic energy cost for bend and twist, respectively. The bend elastic constant can be approximated from the bulk values by $K_{\parallel} \approx \xi K_{\parallel \text{bulk}} d$. The twist constant will be strongly dependent on the tilt angle at the center of the film. For an order-of-magnitude approximation it is given by $K_{\perp} \approx \theta_c^2 K_{\perp \text{bulk}} l$, where θ_c is the tilt angle at the center of the film and l is the distance separating the slabs given by $l = d(N - \xi)$. The third term gives the electrostatic energy within each slab. The fourth term is the electrostatic energy due to charge interactions between the two slabs. H_+ and H_- , are the Hamiltonians for the synclinc and anticlinic arrangements, respectively.

To calculate the free energy, $\Phi(r)$ is rewritten in terms of its Fourier transform $\Phi(q)$. This gives

$$H_{\pm} = \sum_q A(q) [\Phi_1(q)^2 + \Phi_2(q)^2] + B_{\pm}(q) \Phi_1(q) \Phi_2(q), \quad (5)$$

where

$$A(q) = \frac{K_{\parallel}}{2} q^2 + \frac{K_{\perp}}{2l^2} + \frac{P^2}{2\epsilon} \frac{q_x^2}{q}, \quad (6)$$

$$B_{\pm}(q) = \pm \frac{P^2}{2\epsilon} \frac{q_x^2}{q} e^{-ql} - \frac{K_{\perp}}{l^2}. \quad (7)$$

Rewriting the Hamiltonian in terms of normal-mode oscillations gives

$$H_{\pm} = C_{1\pm}(q) \Omega_1(q)^2 + C_{2\pm}(q) \Omega_2(q)^2. \quad (8)$$

Here $C_{1\pm} = A + B_{\pm}/2$, $C_{2\pm} = A - B_{\pm}/2$, $\Omega_1 = (\Phi_1 + \Phi_2)/\sqrt{2}$, and $\Omega_2 = (\Phi_1 - \Phi_2)/\sqrt{2}$.

With this form, the free energy can be expressed as the sum of the contributions from each normal mode. The parameter dependent portion of this sum can be expressed as the following integral:

$$F_{\pm} = \frac{kT}{2} \left(\frac{L}{2\pi} \right)^2 \int dq [\ln(C_{1\pm}) + \ln(C_{2\pm})]. \quad (9)$$

Here L is the film diameter. The free-energy difference between the synclinc and anticlinic arrangements is then given as $\Delta F = F_+ - F_-$. After combining terms and reexpressing the material constants and the integration variable r in unitless forms, this difference is given by

$$\frac{\Delta F}{kT} = \int_0^{2\pi} d\theta \int_1^{r_{\max}} r dr \ln \left(\frac{1 + (a/r)\cos^2\theta(1 + e^{-(r/c)})}{1 + (a/r)\cos^2\theta(1 - e^{-(r/c)})} \right) \times \frac{1 + (b/r)^2 + (a/r)\cos^2\theta(1 - e^{-(r/c)})}{1 + (b/r)^2 + (a/r)\cos^2\theta(1 + e^{-(r/c)})}. \quad (10)$$

Here $a = P^2/(\epsilon K_{\parallel} q_{\min})$, $b = \sqrt{2K_{\perp}/K_{\parallel} l^2 q_{\min}^2}$, $c = 1/(l q_{\min})$, and $r_{\max} = q_{\max}/q_{\min} \cdot q_{\max}$ and q_{\min} are the cutoff frequencies, where $q_{\max} \approx 2\pi/[d \sin(\theta_s)]$ and $q_{\min} = 2\pi/L$. To determine the order-of-magnitude of the fluctuation contribution, the following physical constants are assumed for a 14-layer film of C7: $L = 10^{-2}$ m, $q_{\max} = 2\pi \times 10^{-9}$ m, $P_{fe} = 1.5 \times 10^{-3}$ C/m², $K_{\parallel \text{bulk}} = 10^{-12}$ N, $K_{\perp \text{bulk}} = 10^{-12}$ N, $d = 2.7 \times 10^{-9}$ m, $\theta_c = 0.6^\circ$, and $\xi = 1.5$. The last three parameters are from the fitting parameters given in Fig. 6(b). This gives a value of $\Delta F/kT = 4 \times 10^8$. For comparison, consider that the energy of the interaction of a 10 V/cm electric field and the polarization field for such a film $E_e/kT \cong EPL^2/kT = 1 \times 10^8$ at 70°C. In this model, the fluctuation force driving the film to an anticlinic arrangement is of the same order-of-magnitude as the force of a 10 V/cm electric field driving the film into the synclinic arrangement. This is a reasonable result since the crossover from anticlinic to synclinic for this film occurs at fields of roughly this magnitude.

This model shows that the size of this fluctuation induced free-energy difference is sufficient to induce a synclinic to anticlinic transition. There are a number of inherent uncertainties in this model. For example, θ_c is not well measured by our experiment due to the large uncertainty in ξ . Since the $\Delta F/kT$ goes to zero as θ_c goes to zero, the result is sensitive

to this difficult to measure quantity. Additional parameters could be added to address further details of the system. There is an additional energy cost for changing from the synclinic to the anticlinic arrangement due to the difference between molecular interactions in the synclinic and anticlinic inter-layer interfaces at the center of the film. Additional details could also be added by including the complete twist profile of the film and treating the film as a three-dimensional structure. Ionic impurities could either reduce or enhance the tendency towards antialignment [22]. Such additional parameters, while adding detail to the model, do not further the objective of this paper, which is to provide a simple argument that the fluctuation force is sufficiently large to be considered.

A more extensive investigation into the validity of this model might include a more detailed study of the structure as a function of thickness. Such studies might best be carried using a combination of depolarized light microscopy and ellipsometry. Furthermore, the model predicts quantitatively the increase in fluctuations in the anticlinic arrangement. Measurement of this effect could better test the validity of this model. Such studies may provide much-needed information about the long-range antialigning forces in the tilted smectic phases.

ACKNOWLEDGMENTS

We would like to gratefully acknowledge N. Clark and D. Link for detailed and thought-provoking discussions, and Mr. A. Cady for his help. This research was supported in part by the National Science Foundation, Solid State Chemistry Program, under Grant No. DMR-9703898 and the NATO International Scientific Exchange Program.

-
- [1] K. Binder, in *Phase Transitions and Critical Phenomena*, edited by C. Domb and J.L. Liebowitz (Academic, London, 1986), Vol. 8.
- [2] Ch. Bahr, *Int. J. Mod. Phys. B* **8**, 3051 (1994).
- [3] T. Stoebe and C.C. Huang, *Int. J. Mod. Phys. B* **9**, 2285 (1995).
- [4] P.G. de Gennes and J. Prost, *The Physics of Liquid Crystals*, 2nd ed. (Clarendon Press, Oxford, 1993).
- [5] S. Heinekamp, R.A. Pelcovits, E. Fontes, E.Y. Chen, R. Pindak, and R.B. Meyer, *Phys. Rev. Lett.* **52**, 1017 (1984).
- [6] T. Stoebe, L. Reed, M. Veum, and C.C. Huang, *Phys. Rev. E* **54**, 1584 (1996).
- [7] Ch. Bahr and D. Fliegner, *Phys. Rev. A* **46**, 7657 (1992).
- [8] P.O. Andreeva, V.K. Dolganov, C. Gors, R. Fouret, and E.I. Kats, *Phys. Rev. E* **59**, 4143 (1999).
- [9] D. Schlauf, Ch. Bahr, V.K. Dolganov, and J.W. Goodby, *Eur. Phys. J. B* **9**, 461 (1999).
- [10] D.R. Link, G. Natale, N.A. Clark, J.E. Maclennan, M. Walsh, S.S. Keast, and M.E. Neubert, *Phys. Rev. Lett.* **82**, 2508 (1999).
- [11] R.B. Meyer, L. Liebert, L. Strzelecki, and P. Keller, *J. Phys. (France) Lett.* **36**, 69 (1975).
- [12] R. Bruinsma and J. Prost, *J. Phys. II* **4**, 1209 (1994).
- [13] T. Matsumoto, A. Fukuda, M. Johnno, Y. Motoyama, T. Yui, S. Seomun, and M. Yamshita, *J. Mater. Chem.* **9**, 2051 (1999).
- [14] P.M. Johnson, S. Pankratz, P. Mach, H.T. Nguyen, and C.C. Huang, *Phys. Rev. Lett.* **83**, 4073 (1999).
- [15] R.M.A. Azzam and N.M. Bashara, *Ellipsometry and Polarized Light* (North-Holland, Amsterdam, 1989).
- [16] S. Dumrongrattana, C.C. Huang, G. Nounesis, S.C. Lien, and J.M. Viner, *Phys. Rev. A* **34**, 5010 (1986).
- [17] Ch. Bahr and G. Heppke, *Mol. Cryst. Liq. Cryst.* **150**, 313 (1987).
- [18] Our recent ellipsometric studies on the synclinic and anticlinic arrangements in the compound TFMHPOBC, which shows a bulk $\text{SmC}^* \text{-SmC}_A^*$ transition, suggest that SmC_A^* ordering is present at both surfaces.
- [19] D. Schlauf, Ch. Bahr, and H.T. Nguyen, *Phys. Rev. E* **60**, 6816 (1999).
- [20] D.W. Berreman, *J. Opt. Soc. Am.* **62**, 502 (1972).
- [21] D.R. Link, G. Natale, J.E. Maclennan, N.A. Clark, M. Walsh, S.S. Keast, and M.E. Neubert, *Phys. Rev. Lett.* **83**, 3665 (1999).
- [22] D. R. Link (private communication).